13th ewtec 2019 Proceedings of the 13th European Wave and Tidal Energy Conference 1-6 Sept 2019, Naples, Italy

Moment-Matching-Based Input-Output Parametric Approximation for a Multi-DoF WEC Including Hydrodynamic Nonlinearities

Nicolás Faedo, Yerai Peña-Sanchez, Giuseppe Giorgi and John V. Ringwood

***Abstract*—We present in this paper a moment-matching method to compute a parametric approximation of the input-output (force-to-motion) response of a multiple Degree of Freedom (DoF) Wave Energy Converter (WEC), based on the algorithm presented in [1]. This method allows the user to select a set of interpolation frequencies where the approximating model exactly matches the steady-state response of the target WEC under analysis, while being able to retain key underlying physical properties of the device. Furthermore, we show how to systematically accommodate nonlinear effects using this approximation method, depicting an efficient and versatile approach to compute a parametric representation for WEC design, control and estimation procedures. We illustrate the capabilities and characteristics of this method by means of a study case, using a CorPower-like (heaving point absorber) device. Our numerical analysis shows that, when compared to the currently most-used methodology to parameterise the dynamics of a multi-DoF WEC, the proposed approach can compute mathematical models with the same degree of accuracy and up to $\approx$ 50 % of improvement in terms of computational time.**

***Index Terms*—wave energy, parametric models, force-to-motion, moment-matching, system identification, control**

I. Introduction

WAVE energy design, optimisation and control/estimation procedures virtually always require mathematical models that can represent the intrinsic dynamics of Wave Energy Converters (WECs). These mathematical representations must take into account the underlying trade-off between model accuracy and computational complexity, which is inherently dictated by the particular application being considered. The well-known Boundary Element Method (BEM) is a popular choice to compute the hydrodynamics characteristics of a given WEC device. Though BEM is attractive due to the speed with which numerical simulation may be performed, is inherently limited by the linear nature of potential flow theory, and provides a characterisation of the device in the frequency-domain, i.e. it can only represent the steady-state motion of the WEC. Seeking a more comprehensive approach, the well-known theory developed in [2] expresses the dynamics of a WEC in the time-domain, employing a particular Volterra integro-differential equation of the convolution class. The presence of these convolution terms account for the effect of radiation forces acting on each of the different Degrees of Freedom (DoF) of the device, inherently constituting a hydrodynamic coupling between these modes of motion.

We note that the mere existence of these convolution terms represents a drawback both from a simulation, and a control/estimation theory perspectives. From a pure simulation point of view, it is well-known that the explicit computation of the convolution operator is computationally inefficient, often worsened by the necessity of a small (time) discretisation step to obtain accurate numerical integration. Concerning modern control/estimation techniques, they are virtually always based on the availability of a state-space description (i.e. a set of first order differential equations) of the system under analysis. This also holds in the majority of the literature on wave energy control, which effectively utilise modern optimal control techniques, as reported in, for example, [3].

Motivated by these aforementioned drawbacks, researchers often seek a parametric approximation of this radiation force subsystem in terms of a linear time-invariant system, making explicit use of the hydrodynamic parameters computed with BEM-based codes. To be more precise, the prevailing methodology is to approximate radiation force-related convolution terms as a single-input single-output (SISO) system, even when the problem is inherently of a multiple-input multiple-output (MIMO) nature, as a consequence of the multi-DoF characteristics of the WEC (we note that this MIMO characteristic is also inherently present for the case of arrays of WECs). Examples that consider this approach can be found in [4]–[7], among others. As already noted, in both [1] and [8], this so-called herein "multi-SISO approach" often leads to an unnecessarily high order parameterisation of the radiation force dynamics, potentially rendering any control/estimation strategy unsuitable for real-time applications.

We have recently introduced a moment-matching-based MIMO identification procedure particularly suitable for wave energy applications in [1], based on moment-based theory developed in [9]. This method, which is applied for the first time to a WEC array case (a "farm" of multiple 1-DoF devices), computes a model that *exactly* matches the frequency response of the target MIMO system at a set of user-defined interpolation frequencies $\mathscr{F}$, providing an efficient and accurate method to compute a state-space representation for the WEC dynamics. Motivated by these results, and due to the similarity existing between modeling an array of WECs

Paper ID: 1449. Track: Grid integration, Power take-off and Control (GPC). This material is based upon works supported by Science Foundation Ireland under Grant no. 13/IA/1886.

N. Faedo, Y. Peña-Sanchez and J. V. Ringwood are with the Centre for Ocean Energy Research, Maynooth University, Maynooth, Ireland nicolas.faedo@mu.ie

G. Giorgi is with the Department of Mechanical and Aerospace Engineering, Politecnico di Torino, Turin, Italy.

 Copyright © European Tidal and Wave Energy Conference 2019

and a multi-DoF device, a modification of this algorithm has been presented in [8], which computes a parametric model of the radiation force subsystem of a multi-DoF WEC, with the ability to preserve key physical properties, mainly as a consequence of a sensible selection of the set of interpolation frequencies $\mathscr{F}$. Nevertheless we note that, in [8], we solely discuss the radiation force subsystem, being completely isolated from the WEC input-output (force-to-motion) dynamics, which effectively constitute the relevant system in most of the applications.

In this paper, we propose a method to compute a force-to-motion (i.e. input-output dynamics) parametric representation for a multi-DoF WEC based on moment-matching. We show that, under this moment-based framework, we can compute accurate representations of the force-to-motion behaviour of a WEC with a strong decrease in computational complexity. In addition, we discuss how to accommodate nonlinearities in the obtained moment-based parametric models, such as viscous drag effects and analytical formulations of Froude-Krylov forces [5], leading to nonlinear representations which compute in up to a 60% less time than the method currently implemented in the literature (see, for example, [5]), i.e. the so-called "multi-SISO approach" herein. Furthermore, and unlike the case when the radiation subsystem is parameterised separately, we show that the (local) stability properties of the approximating nonlinear model can be characterised straightforwardly under this input-output moment-based parameterisation framework. Our study case is based on a full-scale multi-DoF CorPower-like device, inspired by the study performed in [5].

The remainder of this paper is organised as follows. Section II introduces the basic concepts behind MIMO moment-based theory, aiming to provide a self-contained study. Section III discusses the basics behind linear modelling of multi-DoF wave energy converters in the time-domain. Section IV elaborates on the moment-based multi-DoF WEC formulation and identification method considered herein. Section V discusses how to accommodate different nonlinear effects in a moment-based parametric description. Finally, Section VI presents the CorPower-like case study, whilst Section VII encompasses the main conclusions of this paper.

A. Notation and Preliminaries

Standard notation is considered through this study, with any exceptions detailed in this section. $\mathbb{R}^+$ ($\mathbb{R}^-$) denotes the set of non-negative (non-positive) real numbers. $\mathbb{C}^0$ denotes the set of pure-imaginary complex numbers and $\mathbb{C}^-$ denotes the set of complex numbers with a negative real part. The symbol 0 stands for any zero element, dimensioned according to the context. The symbol $\mathbb{I}_n$ denotes an order n identity matrix. The spectrum of a matrix $A \in \mathbb{R}^{n\times n}$, i.e. the set of its eigenvalues, is denoted as $\lambda(A)$. The symbol $\bigoplus$ denotes the direct sum of n matrices, i.e. $\bigoplus_{i=1}^{n} A_i = \text{diag}(A_1, A_2, \ldots, A_n)$. The *Kronecker product* between two matrices $M_1 \in \mathbb{R}^{n\times m}$ and $M_2 \in \mathbb{R}^{p\times q}$ is denoted as $M_1 \otimes M_2 \in \mathbb{R}^{np\times mq}$, while the *Kronecker delta* function is denoted as ${}^{i}_{j}\delta$. The convolution between two functions $f(t)$ and $g(t)$ over a finite range $[0, t]$, i.e. $\int_0^t f(\tau)g(t-\tau)d\tau$ is denoted as $f(t) * g(t)$. The space of functions $L^2(\mathbb{R})$ is defined as $L^2(\mathbb{R}) = \left\{ f : \mathbb{R} \to \mathbb{C} | \int_{-\infty}^{\infty} |f(x)^2| dx < \infty \right\}$. The symbol $e^q_{ij} \in \mathbb{R}^{q\times q}$ denotes a matrix with 1 in the ij component and 0 elsewhere. Finally, the symbol $\varepsilon_n \in \mathbb{R}^n$ denotes a vector with odd components equal to 1 and even components equal to 0. In the remainder of this section, the formal definitions of two important operators are presented, since their definition in the literature can often be ambiguous.

Definition 1. [10] (Kronecker sum) *The Kronecker sum between two matrices P_1 and P_2, with $P_1 \in \mathbb{R}^{n\times n}$ and $P_2 \in \mathbb{R}^{k\times k}$, is defined (and denoted) as*

$$P_1 \hat{\oplus} P_2 \triangleq P_1 \otimes \mathbb{I}_k + \mathbb{I}_n \otimes P_2. \tag{1}$$

Definition 2. [10] (Vec operator) *Given a matrix $P = [p_1, p_2, \ldots, p_m] \in \mathbb{R}^{n\times m}$, where $p_j \in \mathbb{R}^n$, $j = 1, \ldots, m$, the vector valued operator vec is defined as*

$$vec\{P\} \triangleq \begin{bmatrix} p_1^\intercal & p_2^\intercal & \ldots & p_m^\intercal \end{bmatrix}^\intercal \in \mathbb{R}^{nm}. \tag{2}$$

II. MIMO MOMENT-BASED THEORY

This section is intended to briefly introduce the reader to the main concepts behind moment-based theory. For a thorough treatment of the underpinning mathematical concepts of this framework, the reader is referred to [11]. We note that the methodology used here was originally developed within the theory of model order reduction.

Consider a finite-dimensional, MIMO, continuous-time system described, for $t \in \mathbb{R}^+$, by the state-space model

$$\begin{aligned} \dot{x}(t) &= Ax(t) + Bu(t), \\ y(t) &= Cx(t), \end{aligned} \tag{3}$$

with $x(t) \in \mathbb{R}^n$, $u(t) \in \mathbb{R}^q$, $y(t) \in \mathbb{R}^p$, $A \in \mathbb{R}^{n\times n}$, $B \in \mathbb{R}^{n\times q}$ and $C \in \mathbb{R}^{p\times n}$. Consider the associated transfer function matrix $W(s) = C(s\mathbb{I}_n - A)^{-1}B : \mathbb{C} \to \mathbb{C}^{p\times q}$ and assume that (3) is minimal.

Definition 3. [12] *The 0-moment of system* (3) *at $s_i \in \mathbb{C}\backslash\lambda(A)$ is the complex matrix $\eta_0(s_i) = C\left(s_i\mathbb{I}_n - A\right)^{-1}B$. The k-moment of system* (3) *at $s_i \in \mathbb{C}$ is the complex matrix*

$$\eta_k(s_i) = \frac{(-1)^k}{k!}\left[\frac{d^k}{ds^k}W(s)\right]_{s=s_i}, \tag{4}$$

with $k \geq 1$ integer.

Moments, as in Definition 3, are the coefficients of the Laurent expansion of the transfer function $W(s)$ about the complex point s_i. That said, we note that the basic idea of the moment-based model order reduction technique is based on interpolating the transfer function of the original system (and the derivatives of this) and the transfer function of the reduced order model (and the derivatives of this) at these specific interpolation points s_i.

The study developed in [13] relates the moments of a SISO linear system to the steady-state output response of the interconnection between an exogenous system (termed *signal generator*), and the dynamical system (3) itself. This same

idea is extended to MIMO systems in [9], and recalled in the following key theorem.

Theorem 1. [9] *Consider system* (3) *and the autonomous multiple-output signal generator*

$$\begin{aligned}\dot{\Xi}(t) &= (\mathbb{I}_q \otimes S)\,\Xi(t),\\ u(t) &= L\,\Xi(t),\end{aligned} \tag{5}$$

with $\Xi(t) \in \mathbb{R}^{q\nu}$, $S \in \mathbb{R}^{\nu\times\nu}$, $L \in \mathbb{R}^{q\times q\nu}$, $\Xi(0) \in \mathbb{R}^{q\nu}$, $\lambda(A) \subset \mathbb{C}^-$, $\lambda(S) \subset \mathbb{C}^0$ *and the eigenvalues of* S *are simple. Suppose the triple of matrices* $(L, \mathbb{I}_q \otimes S, \Xi(0))$ *is minimal. Let* $\Pi \in \mathbb{R}^{n\times q\nu}$ *be the (unique) solution of the Sylvester equation*

$$A\Pi + BL = \Pi(\mathbb{I}_q \otimes S). \tag{6}$$

Then, there exists a one-to-one relation between the moments $\eta_0(s_1)$, $\eta_0(s_2)$, $\ldots$, $\eta_0(s_\nu)$, *with* $s_i \in \lambda(S)$ *for all* $i \in \mathbb{N}_\nu$, *and the steady-state response* $C\Pi\Xi$ *of the output* y *of the interconnection of system* (3) *with the signal generator* (5).

Remark 1. *The minimality of the triple* $(L, \mathbb{I}_q \otimes S, \Xi(0))$ *implies the observability of the pair* $(L, \mathbb{I}_q \otimes S)$ *and the excitability [14] of the pair* $(\mathbb{I}_q \otimes S, \Xi(0))$.

Remark 2. *From now on, we refer to the matrix* $C\Pi \equiv \underline{Y}$, *with* Π *solution of* (6), *as the moment-domain equivalent of* $y(t)$.

Following this steady-state-based interpretation of moments, we now recall from [13] the formal definition of a reduced order model achieving moment-matching for system (3).

Definition 4. [13] *Consider the exogenous signal generator* (5). *The system described by the equations*

$$\begin{aligned}\dot{\Theta}(t) &= F\,\Theta(t) + G\,u(t),\\ \theta(t) &= Q\,\Theta(t),\end{aligned} \tag{7}$$

with $\Theta \in \mathbb{R}^{q\nu}$, $\theta(t) \in \mathbb{R}^p$, $F \in \mathbb{R}^{q\nu\times q\nu}$, $G \in \mathbb{R}^{q\nu\times q}$ *and* $Q \in \mathbb{R}^{p\times q\nu}$ *is a model of system* (3) *at* S *if system* (7) *has the same moments at* S *as system* (3).

Lemma 1. [13] *Consider system* (3) *and the signal generator* (5). *Then, the system* (7) *is a model of system* (3) *at* S *if* $\lambda(F) \cap \lambda(S) = \emptyset$ *and*

$$\underline{Y} = QP, \tag{8}$$

where $\underline{Y} = C\Pi$ *is the moment-domain equivalent of the output of system* (3) *computed from* (6), *and* P *is the unique solution of the Sylvester equation*

$$FP + GL = P(\mathbb{I}_q \otimes S). \tag{9}$$

Remark 3. *The steady-state output of the reduced order model* (7) *exactly matches the steady-state output of the system resulting from the interconnection of system* (3) *and the signal generator* (5).

III. Multi-DoF WECs

The motion for a WEC with N DoF can be expressed in the time-domain according to Newton's second law, obtaining the following hydrodynamic formulation:

$$M\ddot{\chi}(t) = \mathcal{F}_r(t) + \mathcal{F}_h(t) + \mathcal{F}_e(t), \tag{10}$$

where $M = \bigoplus_{i=1}^N m_i$ is the mass matrix of the buoy with m_i the mass of the i-th DoF, and the elements of the vectors $\chi, \mathcal{F}_e, \mathcal{F}_h, \mathcal{F}_r \in \mathbb{R}^N$ contain the excursion $x_i(t)$, excitation force $f_{e_i}(t)$, hydrostatic restoring force $f_{h_i}(t)$ and radiation force $f_{r_i}(t)$ acting on the i-th DoF, with $i \in \mathbb{N}_N$, respectively.

The hydrostatic force $\mathcal{F}_h(t)$ can be written as $-S_h\chi(t)$, where the matrix $S_h \in \mathbb{R}^{N\times N}$ is defined as $S_h = \sum_{i=1}^N \sum_{j=1}^N e_{ij}^N \otimes s_{h_{ij}}$ and contains the hydrostatic stifness of each DoF (if $i = j$) and each interaction between the different modes of motion of the device due to the movement of each respective DoF (if $i \neq j$). The radiation force $\mathcal{F}_r(t)$ is modelled from linear potential theory and, using Cummins' equation [2], is

$$\mathcal{F}_r(t) = -\mu_\infty\ddot{\chi}(t) - \int_0^{+\infty} K(\tau)\dot{\chi}(t-\tau)d\tau, \tag{11}$$

where $\mu_\infty = \lim_{\omega\to+\infty} A(\omega)$, $\mu_\infty > 0$ represents the added-mass matrix at infinite frequency [15] and $K(t) = \sum_{i=1}^N \sum_{j=1}^N e_{ij}^N \otimes k_{ij}(t) \in \mathbb{R}^{N\times N}$, $k_{ij}(t) \in L^2(\mathbb{R})$ contains the (causal) radiation impulse response of each DoF (if $i = j$) and each interaction due to the radiated waves created by the motion of other DoF (if $i \neq j$).

Finally, we can express the linearised equation of motion of the multi DoF WEC as

$$(M + \mu_\infty)\ddot{\chi}(t) + K(t) * \dot{\chi}(t) + S_h\chi(t) = \mathcal{F}_e(t). \tag{12}$$

We note that the internal stability of Equation (12), in the usual Lyapunov sense, has been analysed and guaranteed for any physically meaningful values of the parameters and the mapping $K(t)$ involved [15].

IV. Moment-based WEC formulation

Following [9], we present the motion equation of (12) in a structure more suited to the moment-based theoretical results presented in Section II, i.e.

$$\Sigma : \begin{cases}\dot{\Phi}(t) = A\Phi(t) + B\mathfrak{u}(t),\\ z(t) = \Phi(t),\end{cases} \tag{13}$$

where $\Phi(t) = [\phi_1, \ldots, \phi_N]^\intercal \in \mathbb{R}^{2N}$ is the state-vector of the continuous-time model, with $\phi_i = [x_i(t), \dot{x}_i(t)]^\intercal$. Note that we consider the full state-vector Φ as the output z of (13). The continuous real-valued function $\mathfrak{u}(t) \in \mathbb{R}^N$, described as the input of system (13), is defined as

$$\mathfrak{u}(t) = \mathcal{F}_e(t) - K(t) * (\mathbb{I}_N \otimes [0\ 1])\,\Phi(t). \tag{14}$$

where we note that $(\mathbb{I}_N \otimes [0\ 1])\,\Phi(t) = \dot{\chi}(t)$. Under this assumption, the matrices in (13) can be written in compact form as follows:

$$A = \sum_{i=1}^N \sum_{j=1}^N e_{ij}^N \otimes A_{ij}, \quad B = \sum_{i=1}^N \sum_{j=1}^N e_{ij}^N \otimes B_{ij}, \tag{15}$$

with each $A_{ij} \in \mathbb{R}^{2\times 2}$, $B_{ij} \in \mathbb{R}^2$ defined as

$$A_{ij} = \begin{bmatrix} 0 & {}^i_j\delta \\ -\mathcal{M}_{ij}s_{h_i} & 0 \end{bmatrix}, \quad B_{ij} = \begin{bmatrix} 0 \\ \mathcal{M}_{ij} \end{bmatrix}, \tag{16}$$

where $\mathcal{M}_{ij}$ is the ij-th element of the inverse generalised mass matrix $\mathcal{M} = (M + \mu_\infty)^{-1}$.

Following the theory recalled in Section II, the wave excitation force (input) vector is expressed as a multiple-output implicit form exogenous system as

$$\begin{aligned} \dot{\Xi}_e(t) &= (\mathbb{I}_N \otimes S)\, \Xi_e(t), \\ \mathcal{F}_e(t) &= L_e\, \Xi_e(t), \end{aligned} \tag{17}$$

where the dimension of S is as in Theorem 1, $\Xi_e(t) \in \mathbb{R}^{N\nu}$, $L_e \in \mathbb{R}^{N\times N\nu}$ and, without loss of generality, the initial condition of the signal generator is chosen as $\Xi_e(0) = \varepsilon_{N\nu}$. Given the characteristics of $\lambda(S)$, we consider the finite set $\mathscr{F} = \{\omega_p\}_{p=1}^{f} \subset \mathbb{R}^+$ and write the matrix S in a real block-diagonal form as

$$S = \bigoplus_{p=1}^{f} \begin{bmatrix} 0 & \omega_p \\ -\omega_p & 0 \end{bmatrix}, \tag{18}$$

where $\nu = 2f$, $f \geq 1$ integer. We highlight that, with this particular selection of matrices, the assumption on the minimality of the triple $(L_e, \mathbb{I}_N \otimes S, \Xi_e(0))$ holds as long as the pair $(L_e, \mathbb{I}_N \otimes S)$ is observable.

Remark 4. *Note that each ω_p in* (18) *represents a desired interpolation point for the moment-matching (model reduction) process, i.e. a frequency where the transfer function of the reduced order model matches the transfer function of the original system.*

We now recall a key lemma from [9], which provides a method to compute the moment-domain equivalent of system (13), i.e. the moment-based representation $\underline{Z}$ of the output z.

Lemma 2. [9] *Suppose* (12) *is internally stable in the Lyapunov sense. Then, the moment-domain equivalent $\underline{Z}$ of the output z of system* (13) *can be uniquely determined as*

$$vec\{\underline{Z}\} = \left(\mathbb{I}_N \otimes \Upsilon_\Phi^{\mathscr{R}}\right) vec\{L_e\}, \tag{19}$$

where

$$\begin{aligned} &\Upsilon_\Phi^{\mathscr{R}} = \Upsilon_\Phi^{-1}(\mathbb{I}_\nu \otimes B), \\ &\Upsilon_\Phi = \left(S \hat{\oplus} A\right) + \sum_{i=1}^{N}\sum_{j=1}^{N} \mathscr{R}_{ij}^{\intercal} \otimes -Be_{ij}^{N} \left([1\ 0] \otimes \mathbb{I}_N\right), \end{aligned} \tag{20}$$

with $\Upsilon_\Phi \in \mathbb{R}^{2N\nu\times 2N\nu}$, $\Upsilon_\Phi^{\mathscr{R}} \in \mathbb{R}^{N\nu\times N\nu}$ and where each $\mathscr{R}_{ij} \in \mathbb{R}^{\nu\times\nu}$ is a block-diagonal matrix defined by

$$\mathscr{R}_{ij} = \bigoplus_{p=1}^{f} \begin{bmatrix} {}^{i}_{j}\mathscr{r}_{\omega_p} & {}^{i}_{j}\mathscr{m}_{\omega_p} \\ -{}^{i}_{j}\mathscr{m}_{\omega_p} & {}^{i}_{j}\mathscr{r}_{\omega_p} \end{bmatrix}, \tag{21}$$

with entries depending on the ij-th element of the added mass matrix $A(\omega)_{ij}$ and the radiation damping matrix $B(\omega)_{ij}$ of the device at each specific frequency induced by the eigenvalues of S, as

$${}^{i}_{j}\mathscr{r}_{\omega_p} = B(\omega_p)_{ij}, \quad {}^{i}_{j}\mathscr{m}_{\omega_p} = \omega_p \left[A(\omega_p)_{ij} - \mu_{\infty_{ij}}\right], \tag{22}$$

where $\mu_{\infty ij}$ is the ij-th element of the matrix μ_∞.

Finally, following Definition 4, we define the family of systems achieving moment-matching at the interpolation points specified in the spectrum of S (i.e. the frequencies selected in the set $\mathscr{F}$) as

$$\Sigma \approx \tilde{\Sigma}_{\mathscr{F}} : \begin{cases} \dot{\Theta}(t) = F\Theta(t) + G\mathcal{F}_e(t), \\ \tilde{z}(t) = Q\Theta(t), \end{cases} \tag{23}$$

such that $QP = \underline{\mathcal{V}}$ where P is the unique solution of the Sylvester equation

$$FP + GL_e = P(\mathbb{I}_N \otimes S), \tag{24}$$

and $\underline{Z}$ is the moment-domain equivalent of $z(t) = \Phi(t)$ in (13), computed as in Lemma 2. We note that an appropriate selection of the matrices F, G and Q can be done following the algorithm presented in [9], which effectively combines some of the key results of subspace-based identification methods [16] with moment-based theory. To briefly summarise, the algorithm presented in [9], explicitly uses the frequency-domain data associated with equation (13), which can be readily computed with the output data of BEM codes, i.e. we consider the application of the Fourier transform of (13) to compute the frequency response mapping $H(j\omega)$ between the wave excitation force $\mathcal{F}_e$ and the output Φ, with $H : \mathbb{C}^0 \longrightarrow \mathbb{C}^{2N\times N}$. Then, the matrices F and Q can be approximated using the singular value decomposition of the Hankel matrix associated with the data points $H(j\omega)$ (see [16]). Finally, the input matrix G is obtained by solving for a convex equality-constrained optimisation problem, which minimises the difference between the frequency response of $\tilde{\Sigma}_{\mathscr{F}}$ and the target frequency-domain data of the WEC $H(j\omega)$, while ensuring, at the same time, the moment-matching (interpolation) conditions in (23).

Remark 5. *It is important to note that, using this previously described algorithm, the internal stability of the state-space description obtained can be consistently guaranteed. To be precise, the matrix F in* (23) *can be always selected such that $\lambda(F) \subset \mathbb{C}^-$.*

V. Accomodating nonlinearities

Initially, the motion equation described in state-space (13) are appended with possible nonlinear terms, dependent on both the wave excitation force (input) and the state vector[1], i.e.

$$\Sigma_{nl} : \begin{cases} \dot{\Phi} = A\Phi + B\mathcal{F}_e + B\left(K * (\mathbb{I}_N \otimes [0\ 1])\,\Phi\right) \\ \qquad + Bg(\Phi, \mathcal{F}_e), \\ z = \Phi, \end{cases} \tag{25}$$

where the mapping g accounts for any nonlinear effects acting on the WEC. We assume that $g : \mathbb{R}^{2N} \times \mathbb{R}^N \longrightarrow \mathbb{R}^N$ is such that[2]

$$g(0,0) = 0, \quad \left.\frac{\partial g(\Phi, \mathcal{F}_e)}{\partial \Phi}\right|_{(\Phi,\mathcal{F}_e)=(0,0)} = 0. \tag{26}$$

The practice of parameterising the radiation force convolution operation, separately from the remainder of the WEC dynamics, is often justified (in the wave energy literature) by the fact that is straightforward to accommodate nonlinearities in the differential equation describing the motion of the device,

[1]From now on, we drop the dependence on t when it is clear from context.
[2]Note that this is a standard assumption in nonlinear systems theory [17].

by simply replacing the convolution operation in (25) with its corresponding parametric approximation, and including the mapping g directly in (13). Nevertheless, we note that there is (at least) one substantial downside to this practice: in general, if the convolution term is approximated directly, there is no easy way to assess the stability properties of the resulting system. In other words, even if we approximate the convolution operation with a stable parametric system, there is no guarantee that, when we substitute such a model into (25), the resulting system is Lyapunov stable (unless we can guarantee particular properties on the radiation force approximating model, such as passivity [18], [19]).

That said, the main objective of this section is twofold. Firstly, we show that the moment-based strategy can also be used to accommodate nonlinear effects in a straightforward manner. Secondly, and unlike the case where the radiation force subsystem is approximated separately, we show that we can characterise the stability of the resulting nonlinear system in simple terms, using well-known results from stability theory.

To fulfill our first objective, we use the approximated parametric form (23) to describe the linear behaviour of (25), i.e. we simply construct the interconnected system

$$\Sigma_{nl} \approx \tilde{\Sigma}_{nl_{\mathscr{F}}} : \begin{cases} \dot{\Theta} = F\Theta + G\mathcal{F}_e + Gg(Q\Theta, \mathcal{F}_e), \\ \tilde{z} = Q\Theta = \tilde{\Phi}. \end{cases} \tag{27}$$

System $\tilde{\Sigma}_{nl_{\mathscr{F}}}$ explicitly uses our moment-based approximation of the linear dynamics of the system, i.e. when $g(\cdot,\cdot) = 0$, and provides a parametric description of Σ_{nl}. Aiming to further clarify the underlying principle behind Equation (27), we present a block diagram of both Σ_{nl} and $\tilde{\Sigma}_{nl_{\mathscr{F}}}$ in Figure 1, where we explicitly illustrate the existing interconnection between linear and nonlinear dynamics, showing that the nonlinear mapping can be indeed accommodated in a feedback fashion.

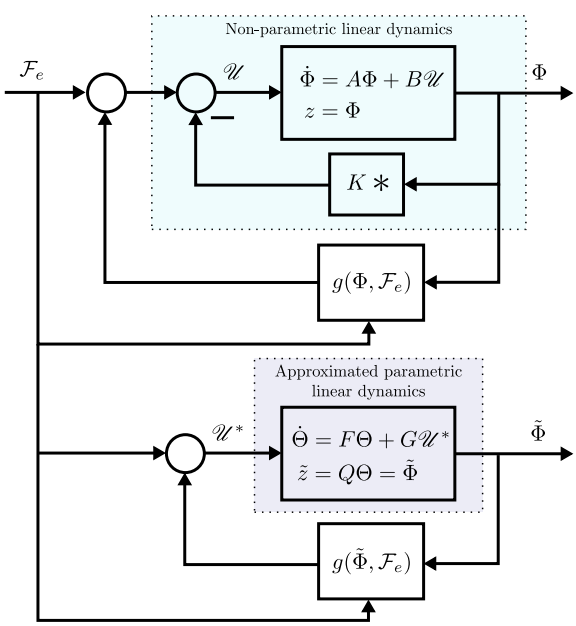

Fig. 1. Block diagram for both Σ_{nl} and $\tilde{\Sigma}_{nl_{\mathscr{F}}}$.

Finally, to accomplish our second objective of assessing the stability of the parametric approximation Σ_{nl}, we formulate the following proposition.

Proposition 1. *Suppose $\mathcal{F}_e(t) = 0$ in (27) and that the dynamic matrix F is such that $\lambda(F) \subset \mathbb{C}^-$. Then, the zero equilibrium of system $\tilde{\Sigma}_{nl_{\mathscr{F}}}$ is locally exponentially stable.*

Proof. Taking into account that the nonlinear mapping g fulfills the conditions expressed in (26), it is straightforward to note that the Jacobian matrix J of system (27) around the equilibrium $(\Theta, \mathcal{F}_e) = (0, 0)$ is given by $J = F$. Then, given that $\lambda(F) \subset \mathbb{C}^-$, $(0, 0)$ is a hyperbolic fixed point, and it follows from Lyapunov's indirect method [17] that the zero equilibrium of system (27) is locally exponentially stable. □

Proposition 1 has a strong impact on the stability assessment of $\tilde{\Sigma}_{nl_{\mathscr{F}}}$: under the presented strategy, the (local) stability properties of the parametric nonlinear system can be fully determined by the moment-based linear approximation (23). In other words, we can always choose $\lambda(F)$ such that the zero equilibrium of the nonlinear system $\tilde{\Sigma}_{nl_{\mathscr{F}}}$ is locally exponentially stable (see Remark 5).

B. Forces depending on the free-surface elevation η

Throughout this paper, we consider the wave excitation force $\mathcal{F}_e(t)$ as the external input to the WEC, merely motivated by its influence (and usage) in the computation of energy-maximising optimal control laws and input-unknown state estimation problems. Though this is, in fact, the usual input selection, we note that our moment-based parameterisation strategy can also be used for the case where the free-surface elevation $\eta(t)$ is chosen as the physical input for the WEC. To be precise, consider the nonlinear system

$$\Sigma_{nl}^{\eta} : \begin{cases} \dot{\Phi} = A\Phi + B(K * (\mathbb{I}_N \otimes [0\ 1])\,\Phi + Bw(\Phi, \eta), \\ z = \Phi, \end{cases} \tag{28}$$

where Φ, A, B and $K(t)$ are defined as in (13), and the mapping $w : \mathbb{R}^{2N} \times \mathbb{R} \longrightarrow \mathbb{R}^N$ accounts for nonlinear effects involving both the state vector Φ and the free-surface elevation η. The function w can be used to represent, for example, nonlinear Froude-Krylov forces (see [5]). Then, we note that the moment-based procedure described in Section IV can be straightforwardly applied to compute a parametric form of the linear behaviour of (28), obtaining the approximating nonlinear system

$$\Sigma_{nl}^{\eta} \approx \tilde{\Sigma}_{nl}^{\eta} : \begin{cases} \dot{\Theta} = F\Theta + Gw(C\Theta, \eta), \\ \tilde{z} = \tilde{\Phi}, \end{cases} \tag{29}$$

where the stability properties of $\tilde{\Sigma}_{nl_{\mathscr{F}}}^{\eta}$ can be assessed following an analogous procedure to that of Proposition 1.

VI. Case Study: a CorPower-like device

We now consider the moment-based identification methodology described previously to obtain finite-order approximating models for a CorPower[3]-like device, as utilised in [5].

[3]See [20] for further up-to-date detail on this particular device.

The device is a heaving point absorber WEC, whose shape and dimensions are based on the study performed in [21] and described herein in Figure 2.

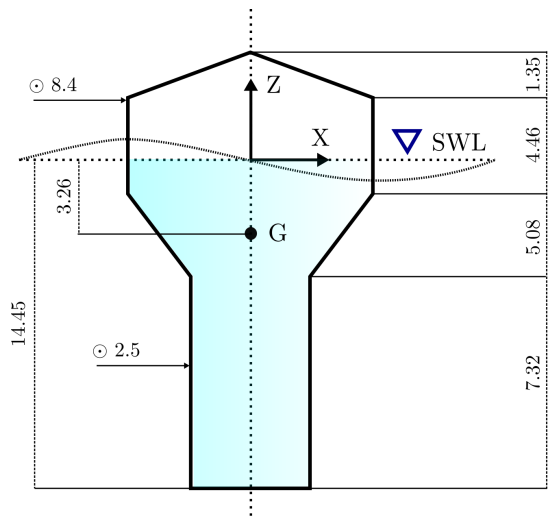

Fig. 2. Schematic of the CorPower-like device.

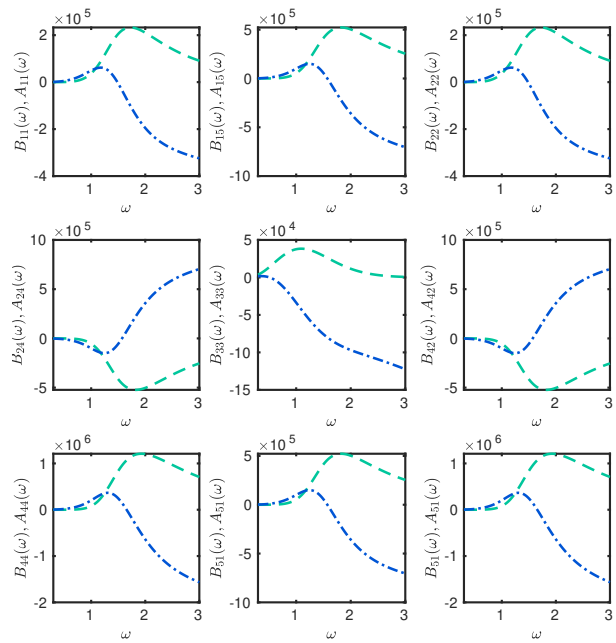

Fig. 3. Hydrodynamic parameters $B(\omega)$ (dashed green) and $A(\omega)$ (dot-dashed blue) for the CorPower-like device.

For this study, we consider five degrees of freedom, i.e $N = 5$ in the equation of motion (12): *surge* (mode 1), *sway* (mode 2), *heave* (mode 3), *roll* (mode 4) and *pitch* (mode 5). We compute the corresponding hydrodynamic coefficients using BEM codes at a finite set of frequencies $\Omega = [0.3, 10]$ with a discretisation step of 0.01 [rad/s]. Nevertheless, we note that ocean wave peak periods typically lie between 3 [s] and 16 [s], which implies that the frequency range that characterises the wave excitation force $\mathcal{F}_e$ is approximately $[0.4, 2.1]$ [rad/s] (see [18]). The radiation damping $B(\omega)$ and radiation added-mass coefficients $A(\omega)$, for this CorPower-like device, can be appreciated in Figure 3. We note that $B_{ii}(\omega), A_{ii}(\omega)$ characterise the radiation force for the i-th degree of freedom (mode), with $i \in \mathbb{N}_5$, while $B_{ij}(\omega), A_{ij}(\omega)$, $i \neq j$, describe the interaction due to radiation effects that mode i exerts on mode j, with $j \in \mathbb{N}_5$. Figure 3 depicts the hydrodynamic coefficients of each characteristic mode, and of those arising from the interactions between modes 1-2, and 2-4. The remaining degrees of freedom do not present interactions due to radiation forces and, hence, they are exactly zero for all $\omega \in \mathbb{R}^+$.

From now on, and following the notation used at the end of Section IV, we denote the frequency-domain equivalent $H(j\omega)$ of the force-to-motion dynamics corresponding to our CorPower-like device as the *target* response. Furthermore, note that each element of the force-to-motion frequency response matrix $H_{ij} : \mathbb{C}^0 \longrightarrow \mathbb{C}$ is the frequency response mapping between the output i, with $i \in \mathbb{N}_{10}$ (position/velocity if i is odd/even, increasingly starting from mode 1), and the input j (excitation force action on the j-th mode). By way of example, $H_{32}(j\omega)$ and $H_{63}(j\omega)$ characterise the effect that the wave excitation force, acting on modes 2 and 3, has on the position of mode 2 and the velocity of mode 3, respectively.

C. Approximation of the force-to-motion response

Following the theory presented herein in Section IV, we now proceed to the explicit computation of a moment-based parametric system $\tilde{\Sigma}_{\mathscr{F}}$, as a function of the target frequency response matrix $H(j\omega)$. A key feature of this moment-matching technique is that the user is allowed to select a set of frequencies $\mathscr{F}$ to interpolate, i.e. where the steady-state response of the approximating model *exactly* matches the target response $H(j\omega)$. For the 1-DoF case (SISO system), a sensible choice can be made by analysing the gain of the target frequency response, and selecting points that characterise dynamically important features. For example, following the discussion in [18], a sensible selection of these interpolation points always includes the resonant frequency of the particular degree of freedom under analysis. We note that this is indeed the frequency where the maximum amplification occurs, i.e $\arg\max_\omega |H(j\omega)|$. For the MIMO case, it is well-known that the corresponding system gain intrinsically depends on the input direction (see [22]), so that the selection of these key dynamical points cannot be performed by simply inspecting each element of $H(j\omega)$ individually. As a matter of fact, the gain of a MIMO system is defined in terms of the singular values of $H(j\omega)$, plotted, for our CorPower-like device case, in Figure 5.

From a straightforward inspection of Figure 5, it is possible to note that both $\omega_1 \approx 0.72$ [rad/s] and $\omega_2 \approx 2.03$ [rad/s] represent dynamically relevant points. We note that the former is the frequency where the maximum input amplification occurs, i.e. the frequency characterising the $\mathscr{H}_\infty$-norm of the system [22]. In fact, ω_1 and ω_2 correspond to the resonant frequency of mode 5 (pitch) and mode 3 (heave), respectively, which are the more dynamically relevant DoFs for this type of device [5].

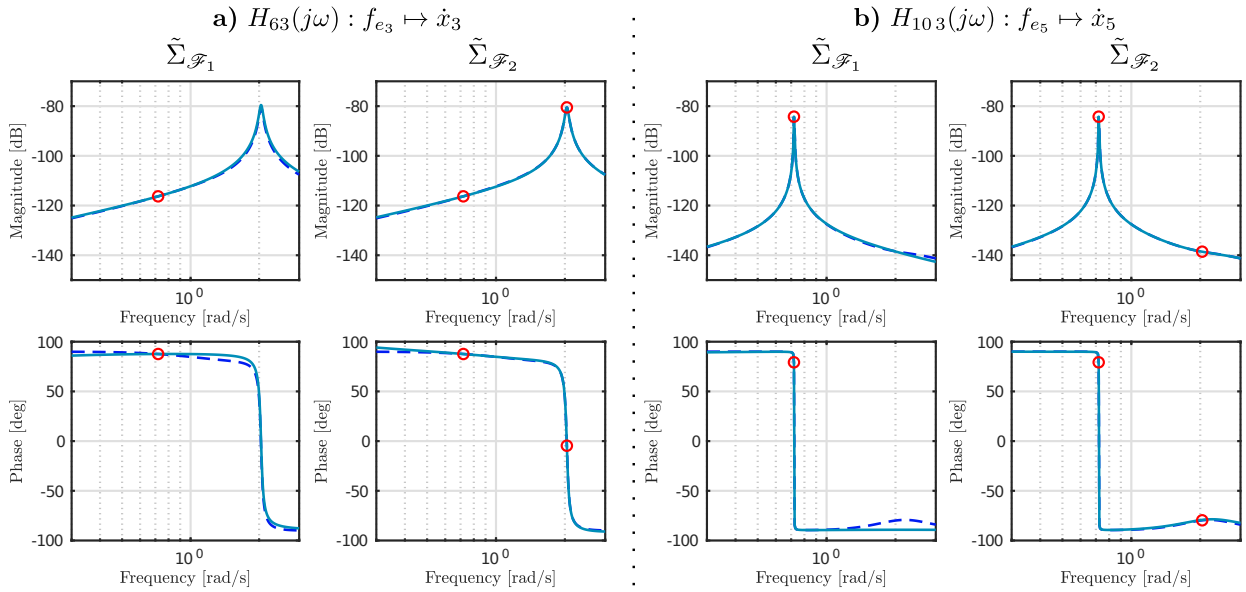

Fig. 4. Bode diagram for the target (dashed blue) frequency-domain elements $H_{63}(j\omega)$ (left, **a**) and $H_{10\,5}(j\omega)$ (right, **b**), along with the corresponding frequency response of each moment-based approximating model (solid green) $\tilde{\Sigma}_{\mathscr{F}_1}$ and $\tilde{\Sigma}_{\mathscr{F}_2}$.

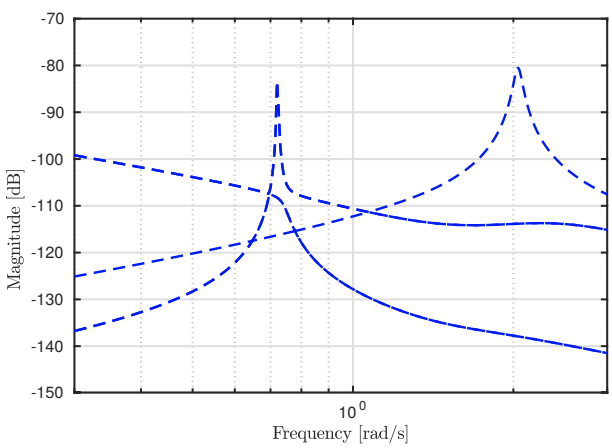

Fig. 5. Singular values plot for the force-to-motion frequency response $H(j\omega)$ of the CorPower-like device.

Following the arguments given in the previous paragraph, we propose two different interpolation sets $\mathscr{F}$:

- $\mathscr{F}_1 = \{0.72\}$,
- $\mathscr{F}_2 = \{0.72, 2.03\}$,

where it is clear that $\mathscr{F}_1 \subset \mathscr{F}_2$. As per discussed in this same section, the frequency range considered to approximate the steady-state behaviour of the target WEC is set to $\Omega_A = [0.3, 3]$ [rad/s], so that the approximating parametric model can successfully characterise the motion of the device in the range where the wave excitation force has significant frequency content (energy-wise).

Due to the fact that heave and surge are the most relevant modes of motion for this particular CorPower-like device, Figure 4 shows the Bode diagram for the elements $H_{63}(j\omega)$ (left, **a**) and $H_{10\,5}(j\omega)$ (right, **b**), i.e. the target frequency-response of modes 3 (heave) and 5 (surge) considering velocity as output, along with the corresponding frequency response of each moment-based approximating model $\tilde{\Sigma}_{\mathscr{F}_1}$ and $\tilde{\Sigma}_{\mathscr{F}_2}$. We note that the interpolation frequencies selected for the computation of each parametric model, i.e. the elements of the sets $\mathscr{F}_1$ and $\mathscr{F}_2$, are denoted in Figure 4 using an empty red circle. It can be readily appreciated that, by a sensible selection of the interpolation frequency set $\mathscr{F}_1$, the approximating model $\tilde{\Sigma}_{\mathscr{F}_1}$ provides an accurate frequency-domain description when compared with the target steady-state response of the WEC under analysis. Note that the steady-state response of the parametric model *exactly* matches the steady-state response of the CorPower-like device for the frequencies selected in each set $\mathscr{F}$. The overall approximation offered by $\tilde{\Sigma}_{\mathscr{F}_1}$ can be further improved by proposing a parametric model matching the set $\mathscr{F}_2$, which includes the resonant frequencies of both heave and pitch modes as interpolation points, as can be appreciated in Figure 4. As discussed previously, in this section, frequency-domain analysis of a MIMO system can be carried out accurately in terms of the singular value decomposition of its frequency-response matrix $H(j\omega)$. That said, and as a conclusive graphical illustration of the frequency-domain performance of the parametric models computed using our moment-based strategy, Figure 6 depicts the singular values plot for the target response $H(j\omega)$, along with the corresponding singular value analysis of the approximating models $\tilde{\Sigma}_{\mathscr{F}_1}$ and $\tilde{\Sigma}_{\mathscr{F}_2}$. One can straightforwardly appreciate that both moment-based models can accurately describe the target MIMO gain in every principal direction, with a decrease in approximation error when going from $\tilde{\Sigma}_{\mathscr{F}_1}$ (parametric system of dimension 10) to $\tilde{\Sigma}_{\mathscr{F}_1}$ (parametric system of dimension 20).

To give a precise measure of the frequency-domain performance of both moment-based parametric approximations $\tilde{\Sigma}_{\mathscr{F}_1}$ and $\tilde{\Sigma}_{\mathscr{F}_2}$, Table I offers a numerical comparison in terms of the following key indicators:

- **Dim**: Order of the approximating parametric model.

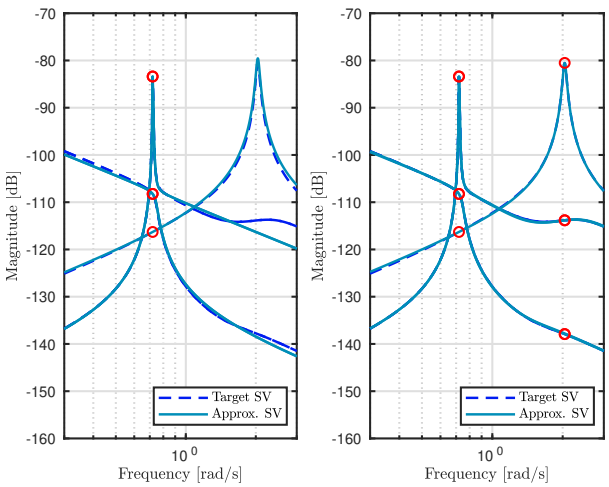

Fig. 6. Singular values values plot for the force-to-motion frequency response $H(j\omega)$ of the CorPower-like device considered in this study, along with the corresponding singular value analysis of both approximating models $\tilde{\Sigma}_{\mathscr{F}_1}$ (left) and $\tilde{\Sigma}_{\mathscr{F}_2}$ (right).

- **NRMSE$_\mathbf{F}$**: Normalised Root Mean Square Error (NRMSE) computed against the target WEC force-to-motion frequency response $H(j\omega)$, with $\omega \in \Omega_A$.

Model	Dim	NRMSE$_\mathbf{F}$
multi-SISO approach	46	0.91%
$\tilde{\Sigma}_{\mathscr{F}_1}$	10	5.89%
$\tilde{\Sigma}_{\mathscr{F}_2}$	20	0.97%

TABLE I. Numerical appraisal of the moment-based parametric models with regard to their frequency-domain performance.

We note that the first row of Table I includes what we call the "SISO approach", which essentially constitutes a parametric model of the WEC system (13) obtained by approximating each individual convolution operation with a SISO system, i.e. in a decoupled manner. As discussed in Section I, this is indeed the most common methodology in the literature, and is included in Table I for comparison. In this paper, the strategy used to compute an approximation of each of this convolution terms separately, is the SISO moment-matching method[4] described in [18] (with $\mathscr{F}_2$ as interpolation points), resulting in an input-output state-space description for (13) of dimension 46.

As can be appreciated directly from Table I, the moment-based parametric model $\tilde{\Sigma}_{\mathscr{F}_1}$ already provides quite accurate results, with a NRMSE of less than 6% for the frequency range of interest. This performance can be further improved by considering the parametric approximation $\tilde{\Sigma}_{\mathscr{F}_2}$, which performs with $\approx$ 99% of accuracy inside the set Ω_A. It is noteworthy to highlight that the so-called 'multi-SISO approach' provides similar frequency-domain performance to that of $\tilde{\Sigma}_{\mathscr{F}_2}$, but with higher model complexity (i.e. higher model order). The impact of this increase in model order, in terms of computational requirements, is further analysed in the following subsection, where we consider the inclusion of nonlinear effects in the WEC dynamical model.

D. Accommodating nonlinear effects

Following Section V, we now consider nonlinear effects in the WEC model, as specifically expressed in system Σ_{nl} (see Equation (25)). To begin this analysis, we assume that the nonlinear mapping g accounts for the viscous drag effects acting on the WEC, which can be written, according to the well-known Morison equation [24], as

$$g(\mathcal{F}_e, \Phi) = g(\Phi) = -b_d \left|\dot{\chi}\right| \dot{\chi}, \tag{30}$$

where we recall that $(\mathbb{I}_N \otimes [0\ 1])\,\Phi = \dot{\chi}$ and $b_d \in \mathbb{R}^+$ is a constant coefficient[5]. To assess the performance of the moment-based parametric models, when it comes to accommodating nonlinear effects, we construct the approximating systems $\tilde{\Sigma}_{nl_{\mathscr{F}_1}}$ and $\tilde{\Sigma}_{nl_{\mathscr{F}_2}}$ as in Equation (27), i.e. based on the same approximations computed in Section VI-C. Table II offers a numerical performance appraisal using similar indicators to those of Table I, i.e.:

- **Dim**: Order of the approximating parametric model.
- **NRMSE$_\mathbf{T}$**: NRMSE computed (in steady-state) against the target time-domain response computed directly from Σ_{nl} (i.e. explicitly solving each corresponding convolution integral). Irregular incident waves with an angle of attack of 45° are generated using a JONSWAP spectrum[6] with significant frequency content inside the set Ω_A.
- **S-Time**: time required for 150 [s] of time-domain simulation, averaged over 100 simulation cases.
- **T-Gain**: % of improvement in **S-Time** with respect to the slowest model (*benchmark*).

We note that, to get meaningful results for the time-domain scenario presented in Table II, and since the inputs are generated from sets of random amplitudes, it is found that the mean of 10 simulations is necessary to obtain a 95% confidence interval with a half-width of 0.25% of the mean, computed as in [7]. To assess the computational requirements

Model	Dim	NRMSE$_\mathbf{T}$	S-Time	T-Gain
multi-SISO approach	46	1.29%	3.46[s]	*Benchmark*
$\tilde{\Sigma}_{\mathscr{F}_1}$	10	9.94%	1.91[s]	44.91%
$\tilde{\Sigma}_{\mathscr{F}_2}$	20	2.06%	2.12[s]	38.84%

TABLE II. Numerical appraisal of the moment-based parametric models with regard to their time-domain performance (including nonlinearities).

of each model, the totality of the simulations are carried out

[4]We note that this strategy is implemented in a MATLAB-based application called FOAMM, which can be directly downloaded from [23]

[5]We do not discuss herein the determination of a fixed value for this constant coefficient. The reader is referred to [25] for a thorough treatment of this topic.

[6]Significant wave height $H_s = 1.5$ [m], Peak period $T_p = 8$ [s] and peak enhancement factor $\gamma = 3.3$ (see [26]).

utilising the MATLAB built-in function *ode45* (explicit Runge-Kutta method). Similarly to the frequency-domain analysis of Section VI-C, Table II also includes the so-called "multi-SISO approach", which is essentially Σ_{nl} with each convolution term approximated independently.

Inspecting the results of Table II, it is noteworthy that the moment-based parametric model $\tilde{\Sigma}_{nl_{\mathscr{F}_2}}$ presents a similar accuracy to that of the multi-SISO approach, with the former computing in almost 40% less time than the latter. We emphasize the importance of this last statement given that, for almost the same degree of model accuracy, the moment-based approximating model $\tilde{\Sigma}_{nl_{\mathscr{F}_2}}$ computes significantly faster than the usual approach utilised in the literature (i.e. the "multi-SISO approach"), being specially suited for any nonlinear WEC control/estimation applications. With regards to $\tilde{\Sigma}_{nl_{\mathscr{F}_1}}$, though this system presents a NRMSE of approximately 10%, it is more computationally efficient than the remainder of the models. That said, we note that the utility of such a (low order) representation depends heavily on the trade-off between computational cost and accuracy required by the application.

As a graphical illustration of the time-domain performance of the moment-based models computed herein, Figure 7 (left axis) offers the time-domain (velocity) response of $\tilde{\Sigma}_{nl_{\mathscr{F}_2}}$, along with the corresponding target time-domain response for the CorPower-like device directly computed from Σ_{nl}. The right axis of Figure 7 shows the exact excitation force input used to elicit such a response, for each of the DoF considered. It is straightforward to appreciate from Figure 7 that each of the outputs of the approximating model $\tilde{\Sigma}_{nl_{\mathscr{F}_2}}$ behaves almost identically to its corresponding target output computed from Σ_{nl}, agreeing with the results presented in Table II.

To finalise this case of analysis, we now consider nonlinearities which intrinsically depend on the free-surface elevation η, as described in Section V-B by means of the mapping $\omega(\Phi, \eta)$. In particular, we include both viscous drag effects (as in Equation (30)) and nonlinear Froude-Krylov (FK) forces, which represent the integral of the static and dynamic pressure over the wetted surface of the device. We note that, as discussed in [27], these nonlinear effects are especially important for heaving point absorbers, such as the CorPower-like device analysed herein. To include FK forces in both Σ_{nl}^{η} and $\tilde{\Sigma}_{nl_{\mathscr{F}}}^{\eta}$ (see Equation (28) and (29), respectively), we utilise the computationally efficient analytical approach developed in [5], which avoids the time-consuming mesh-based approaches by solving FK forces algebraically[7]. Aiming to assess the performance of the moment-based model $\tilde{\Sigma}_{nl_{\mathscr{F}_2}}^{\eta}$, Table III offers an analogous analysis to that of Table II, where now the so-called "target" response, considered for the computation of the corresponding NRMSE, is obtained directly from Σ_{nl}^{η}. We note that for this FK forces case, we only analyse regular incident waves as inputs, with 1 [m] height and an angle of attack of $0°$, hence the generalised drop in computational time (**S-Time**) with respect to Table II.

Table III provides a strong conclusion: a wise parameterisation of the input-output dynamics provides almost the same degree of accuracy as the currently utilised method, with an improvement in computational time of $\approx 47\%$ (almost half of the computational requirements to those of the multi-SISO approach). This directly implies that the computationally efficient approach to compute nonlinear FK forces presented in [5] can be further improved by simply changing the system parameterisation approach, i.e. using our moment-based model $\tilde{\Sigma}_{nl_{\mathscr{F}_2}}$. To finalise the results presented in this section, Figure 8 illustrates the time-domain velocity for the three excited DoF (modes 1,3 and 5), for both the target response computed from Σ_{nl}^{η} and the parametric representation $\tilde{\Sigma}_{nl_{\mathscr{F}_2}}^{\eta}$.

[7]We note that this algebraic approach relies on the assumption of small pitch (mode 5) angles (see [5]).

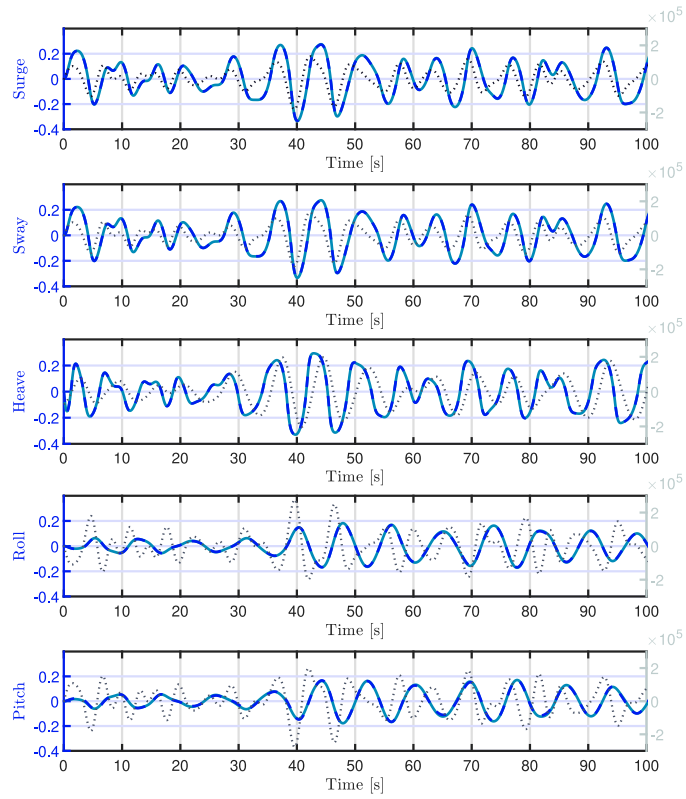

Fig. 7. Time-domain response (velocity) of the parametric model $\tilde{\Sigma}_{nl_{\mathscr{F}_2}}$ (solid green), along with the corresponding target time-domain response computed from Σ_{nl} (dashed blue). The right axis shows the wave excitation force input used to simulate such a response, for each of the DoF considered.

Model	**Dim**	**NRMSE$_T$**	**S-Time**	**T-Gain**
multi-SISO approach	46	1.10%	0.66[s]	*Benchmark*
$\tilde{\Sigma}_{\mathscr{F}_2}^{\eta}$	20	3.67%	0.35[s]	46.97%

TABLE III. Numerical appraisal of the moment-based parametric models with regard to their time-domain performance (including nonlinearities depending on η).

VII. CONCLUSIONS

This paper utilises a moment-based approach to compute a MIMO parametric approximation of the linear force-to-motion (i.e. wave excitation force to position/velocity variables) response of a multiple-DoF WEC. We show that this particular

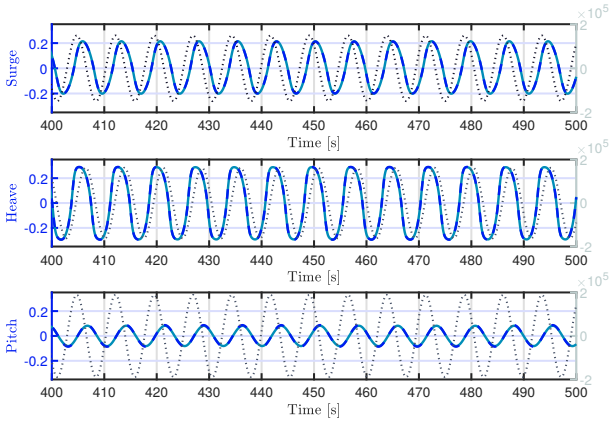

Fig. 8. Time-domain response (velocity) of the parametric model $\tilde{\Sigma}^{\eta}_{nl_{\mathscr{F}_2}}$ (solid green), along with the corresponding target time-domain response computed from Σ^{η}_{nl} (dashed blue). The right axis shows the wave excitation force input used to simulate such a response, for each of the DoF considered.

methodology presents several advantages, including both the possibility of ensuring internal stability of the parametric model, and of choosing a set of frequencies where the steady-state response of the obtained approximating system *exactly* matches the steady-state response of the WEC under analysis. We show that a sensible selection of this set of key frequencies provides an accurate approximation, while preserving additional properties such as, for example, the $\mathscr{H}_\infty$-norm of the target system. We also discuss herein how to accommodate different types of nonlinearities on the presented parametric models, leading to accurate and computationally efficient nonlinear representations. Moreover, we show that, with the methodology proposed, the assessment of the (local) stability properties of the resulting nonlinear parametric model can be determined in terms of the moment-based approximation of its corresponding linear dynamics.

We assess the performance of the strategy on a CorPower-like device, inspired by [5]. We first show that the frequency-domain performance of the computed parametric models can accurately represent the target WEC, with a NRMSE of less than 1% when two (key) frequencies are selected as interpolation points. Later on, we illustrate how to accommodate nonlinear effects in the time-domain, including viscous forces and Froude-Krylov forces. Numerical results show that our moment-based method provides a nonlinear parametric model with a NRMSE (in time-domain) of $\approx 2\%$, while improving in almost 50% the computational efficiency obtained with the methodology currently implemented in the literature, making this framework appealing for real-time applications.

ACKNOWLEDGMENT

This material is based upon works supported by Science Foundation Ireland under Grant no. 13/IA/1886.

REFERENCES

[1] Y. Peña-Sanchez, N. Faedo, and J. V. Ringwood, "Moment-based parametric identification of arrays of wave energy converters," in *2019 American Control Conference (ACC), Philadelphia (Accepted)*, 2019.

[2] W. E. Cummins, "The impulse response function and ship motions," *Schiffstechnik*, vol. 47, pp. 101–109, 1962.

[3] N. Faedo, S. Olaya, and J. V. Ringwood, "Optimal control, MPC and MPC-like algorithms for wave energy systems: An overview," *IFAC Journal of Systems and Control*, vol. 1, pp. 37–56, 2017.

[4] G. Li and M. R. Belmont, "Model predictive control of sea wave energy converters–part i: A convex approach for the case of a single device," *Renewable Energy*, vol. 69, pp. 453–463, 2014.

[5] G. Giorgi and J. V. Ringwood, "A compact 6-dof nonlinear wave energy device model for power assessment and control investigations," *IEEE Transactions on Sustainable Energy*, vol. 10, no. 1, pp. 119–126, 2019.

[6] J. Hals, J. Falnes, and T. Moan, "Constrained optimal control of a heaving buoy wave-energy converter," *Journal of Offshore Mechanics and Arctic Engineering*, vol. 133, no. 1, p. 011401, 2011.

[7] Y. Peña-Sanchez, M. Garcia-Abril, F. Paparella, and J. V. Ringwood, "Estimation and forecasting of excitation force for arrays of wave energy devices," *IEEE Transactions on Sustainable Energy*, 2018.

[8] N. Faedo, Y. Peña-Sanchez, and J. V. Ringwood, "Parameterisation of radiation forces for a multiple degree of freedom wave energy converter using moment-matching: a case study." in *2019 ISOPE conference, Hawaii (under review)*, 2019.

[9] N. Faedo, G. Scarciotti, A. Astolfi, and J. V. Ringwood, "Moment-based constrained optimal control of an array of wave energy converters," in *2019 American Control Conference (ACC), Philadelphia (Accepted)*, 2019.

[10] J. Brewer, "Kronecker products and matrix calculus in system theory," *IEEE Transactions on circuits and systems*, vol. 25, no. 9, pp. 772–781, 1978.

[11] G. Scarciotti and A. Astolfi, "Nonlinear model reduction by moment matching," *Foundations and Trends in Systems and Control*, vol. 4, no. 3-4, pp. 224–409, 2017.

[12] A. C. Antoulas, *Approximation of large-scale dynamical systems*. SIAM, 2005.

[13] A. Astolfi, "Model reduction by moment matching for linear and nonlinear systems," *IEEE Transactions on Automatic Control*, vol. 55, no. 10, pp. 2321–2336, 2010.

[14] A. Padoan, G. Scarciotti, and A. Astolfi, "A geometric characterization of the persistence of excitation condition for the solutions of autonomous systems," *IEEE Transactions on Automatic Control*, vol. 62, no. 11, pp. 5666–5677, 2017.

[15] J. Falnes, *Ocean waves and oscillating systems: linear interactions including wave-energy extraction*. Cambridge university press, 2002.

[16] T. McKelvey, H. Akçay, and L. Ljung, "Subspace-based multivariable system identification from frequency response data," *IEEE Transactions on Automatic Control*, vol. 41, no. 7, pp. 960–979, 1996.

[17] H. K. Khalil, *Noninear Systems*. Prentice-Hall, New Jersey, 1996.

[18] N. Faedo, Y. Peña-Sanchez, and J. V. Ringwood, "Finite-order hydrodynamic model determination for wave energy applications using moment-matching," *Ocean Engineering*, vol. 163, pp. 251 – 263, 2018.

[19] N. Faedo, Y. Peña Sanchez, and J. V. Ringwood, "Passivity preserving moment-based finite-order hydrodynamic model identification for wave energy applications," in *Advances in Renewable Energies Offshore, RENEW 2018*, 2018, pp. 351–359.

[20] CorPower, *The CorPower Wave Energy Converter*, 2019, accessed January 10. [Online]. Available: http://www.corpowerocean.com/

[21] J. H. Todalshaug, G. S. Asgeirsson, E. Hjálmarsson, J. Maillet, P. Möller, P. Pires, M. Guérinel, and M. Lopes, "Tank testing of an inherently phase-controlled wave energy converter," *International Journal of Marine Energy*, vol. 15, pp. 68–84, 2016.

[22] K. Zhou and J. C. Doyle, *Essentials of robust control*. Prentice hall Upper Saddle River, NJ, 1998, vol. 104.

[23] Centre for Ocean Energy Research, Maynooth University, *FOAMM Toolbox*, 2019, accessed January 10. [Online]. Available: http://www.eeng.nuim.ie/coer/downloads/

[24] J. Morison, J. Johnson, S. Schaaf *et al.*, "The force exerted by surface waves on piles," *Journal of Petroleum Technology*, vol. 2, no. 05, pp. 149–154, 1950.

[25] G. Giorgi and J. V. Ringwood, "Consistency of viscous drag identification tests for wave energy applications," in *Proceedings of the 12th European Wave and Tidal Energy Conference (EWTEC). Cork*, 2017.

[26] K. Hasselmann, "Measurements of wind wave growth and swell decay during the Joint North Sea Wave Project (JONSWAP)," *Dtsch. Hydrogr. Z.*, vol. 8, p. 95, 1973.

[27] G. Giorgi and J. V. Ringwood, "Comparing nonlinear hydrodynamic forces in heaving point absorbers and oscillating wave surge converters," *Journal of Ocean Engineering and Marine Energy*, vol. 4, no. 1, pp. 25–35, 2018.